ABSTRACT:

The intent of this document is to summarise early stages of a personal research exercise that ultimately aims to assist the application of the author's no-moving-part Fluidics technology experience to a new Third-Generation Fluidics (3GF) approach with an aim to meet the requirements of nuclear and wider applications and industries. The work introduced in this document is centred on the author's 40 years of research and application experience in the generic field of Fluidics and his new interests in Computational Fluid Dynamics (CFD).

Fluidic no-moving-part technology has provided small Signal Fluidic (SF) and larger Power Fluidic (PF) devices. Power Fluidics has been used and is still being applied to handling systems in the UK and USA nuclear industries and the author has also applied it to UK Chemical, Pharmaceutical and Oil & Gas industries.

The work described here introduces investigations conducted using Computational Fluid Dynamics (CFD) on a model of a historic PF device known as a Vortex Amplifier (VXA). It is intended to gain confidence in CFD suitability and confirm its applicability to the historic VXA.

Following a brief introduction to the approach, observations obtained from CFD modelling of the historic VXA design and recommendations of the next steps to be taken are discussed.

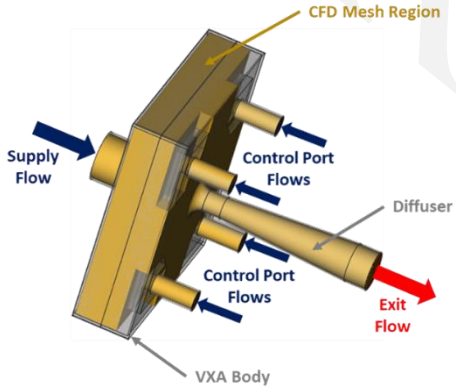

The VXA CFD Model

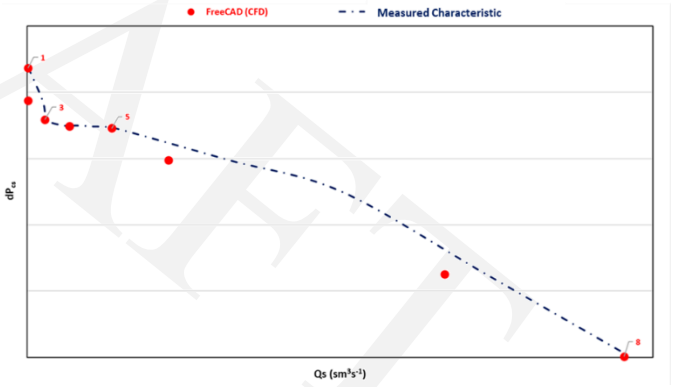

The CFD and Measured VXA Characteristics

The above CFD model was prepared in open-source 3D drafting, CFD modelling and data assessment software and resulted in the above characteristics that have confirmed that the CFD model is providing excellent results. The modeling has also provided the following valuable indications of key velocity vector areas that provided the above characteristic.

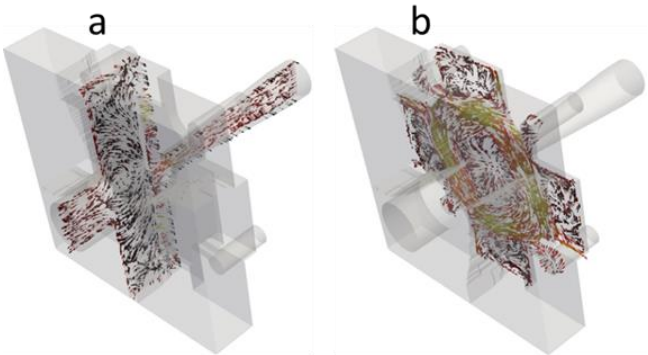

Axial Velocity Plane **Chamber Velocity Plane**

CFD Model Velocity Vector Planes

Preliminary Computational Fluid Dynamic Modeling Of A Historic Vortex Amplifier

M. J Crossley
The Vortex Chamber
Tinsley Barn
Dockinsall Lane
Out Rawcliffe
Lancashire
PR3 6TE
mcrossleyuk@gmail.com

February 2022

INTRODUCTION

A main objective of this document has been to provide the opportunity for the author to gather brief observations that have been made from recent Computation Fluid Dynamics (CFD) assessments. The assessment has been conducted on a Complete 300mm Vortex Amplifier (VXA) model. This complete model comprised of a full geometric 3D model of the VXA body and contents that also included a 3D CFD mesh that represented all internal flow paths. This complete model is illustrated below. The intention of this note was originally merely to provide the author a tool to record and aid his understanding of his CFD observations but has turned out to be very helpful.

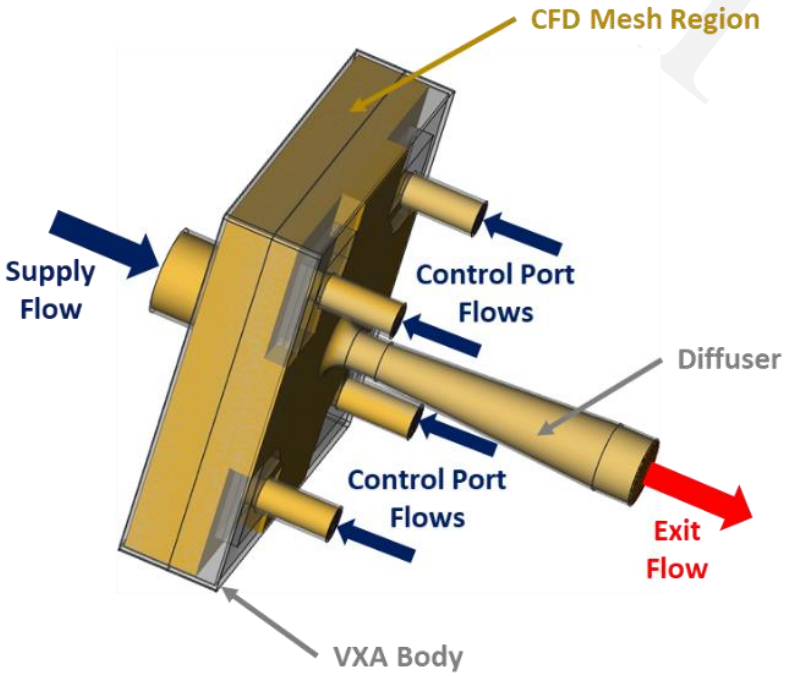

Figure 1 – Complete VXA Geometric Mesh

The work briefly introduced in this document is centred on the author's 40 years of research experience in the field of Fluidics. Fluidic technology was introduced during the 1950s as Signal Fluidics (SF) that provided logic circuits that were used to control fuel flow in rockets, using small fluid control devices with no-moving-parts. During the 1970s the author commenced his research into the second generation of fluidics that has been termed Power Fluidics (PF).

As these terms suggest, the same no-moving-part technology has therefore provided small Signal Fluidic and larger Power Fluidic devices. Power Fluidics is still being used in process systems in the UK and USA nuclear industries. The author has also utilised Power Fluidic technology in the UK Chemical, Pharmaceutical and Oil & Gas industries.

Power Fluidic technology has been utilised widely in the UK nuclear industry and latterly in the USA. It has provided no-moving-part technology for use in:

- Nuclear fuel fabrication plant ventilation systems
- Spent nuclear fuel recovery and reprocessing plants.
- Materials handling in chemical and pharmaceutical facilities

This no-moving-part technology has provided a significant reduction in maintenance requirements providing safer and longer component and plant operating life.

The author is intending to investigate a Third Generation Fluidic (3GF) approach that will be built upon the work discussed in this document. This document centres on a Fluidic element that has historically been identified as a Vortex Amplifier (VXA) that is introduced and described below.

THE VORTEX AMPLIFIER (VXA)

The Vortex Amplifier (VXA) is a three-port no-moving-part device that utilises an internally generated vortex flow to restrict and regulate flow and pressure. The simplest, generic, form of a VXA is illustrated below.

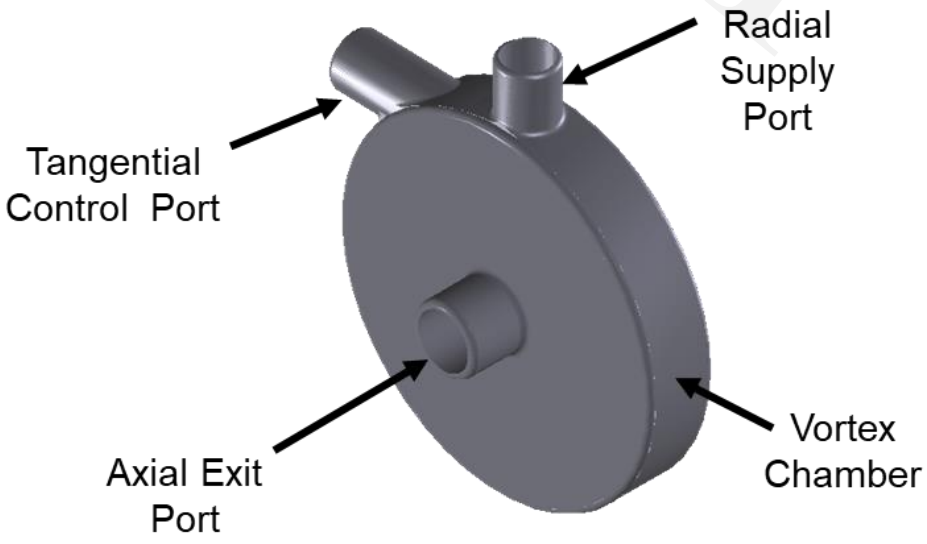

Figure 2 – Vortex Amplifier Generic Concept

The generic VXA illustrated in Figure 2 consists of a simple narrow cylinder, known as the vortex chamber, that has radial and tangential inlet ports and a single axial exit port.

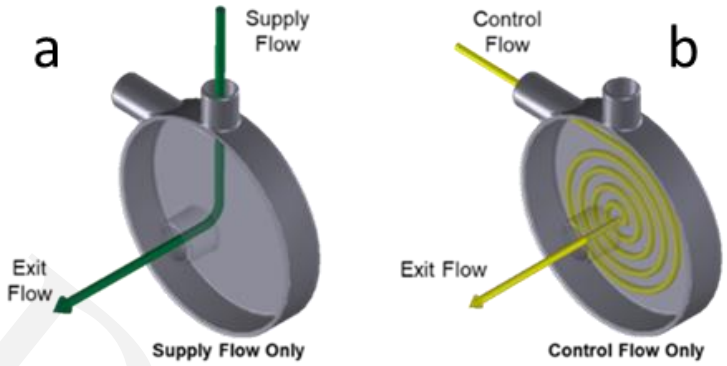

Figure 3 – Generic VXA Inlet and Exit Flow Paths

In Figure 3(a), Fluid entering the vortex chamber via the radial supply port can leave via the axial exit port with little restriction to flow. In Figure 3(b), the vortex chamber geometry forces flow entering via the tangential control port to generate a vortex before exiting via the exit port; resulting in a significantly greater resistance to flow and hence pressure drop.

Let us now consider an application for the VXA that is of particular interest here. This VXA has been used to regulate the flows and pressures within hazardous material handling enclosures and in particular nuclear Gloveboxes.

A simplified arrangement of a VXA and nuclear handling glovebox enclosure is diagrammatically illustrated below.

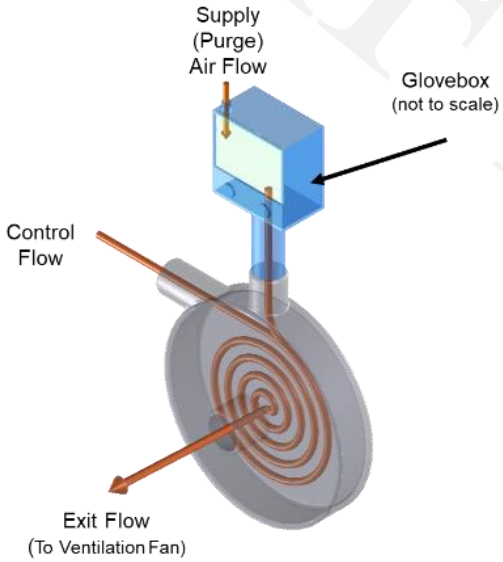

Figure 4 – Glovebox and Generic VXA

Figure 4 illustrates an unscaled representation of a Glovebox Enclosure and the generic VXA with its now combined supply and control flow paths. The VXA supply flow is now the purge flow entering and leaving the glovebox. The tangential control flow is combining with the supply flow, generating a vortex in the vortex chamber. Both these flows are generated by the reduced pressure generated by the downstream ventilation fan.

In this case, the control flow is drawn from the external atmosphere. The fan depression that is drawing airflow into the glovebox and VXA has historically been assumed to be a negative pressure in the order of -1500Pag and atmospheric pressure is taken to be 0Pag. As a result, these two pressures and resulting flows define the VXA's operating condition.

The vortex generated in the vortex chamber and hence resulting pressure drop is limiting the flow from the glovebox and regulating the pressure at the supply port and hence inside the glovebox. It is aimed to maintain a maximum constant glovebox depression to a value in the order of -200Pag in order to maintain comfortable operating conditions for the operator using the glovebox gloves.

The condition that is of concern for all hazardous material handling enclosures, such as the glovebox, is a breach, i.e., a break in the enclosure containment resulting in the risk of hazardous materials leaving and entering the operating area. In the glovebox case, the most likely large breach is the loss of a single glove.

Such a breach results in the glovebox pressure climbing towards the operating area's atmospheric pressure. The breach therefore removes the pressure difference between the glovebox and control port inlet, that is also assumed to be at atmospheric pressure. Removal of this pressure difference reduces or eliminates the tangential control flow into the vortex chamber and dramatically reduce the strength of the vortex. This results in a condition close to the supply flow only condition illustrated in Figure 3(a) above. The VXA may now be regarded as being in an almost open maximum flow condition.

This breach condition therefore results in maximum airflow drawn into the glovebox via the breach and the fan is sized to provide a breach flow of sufficient magnitude to generate a minimum velocity in the breach of $1ms^{-1}$. A safe operating condition is therefore automatically maintained under normal and hazardous failure conditions.

The simple generic VXA introduced above could not meet the demands of glovebox enclosure requirements. As a result, a more complex VXA was developed in the 1970s to meet operational demands and aid inclusion in nuclear industry glovebox suites. The resulting VXA design is introduced below.

This now historic VXA has a more complex geometry than the generic device that is illustrated in Figure 4 above and is now illustrated below.

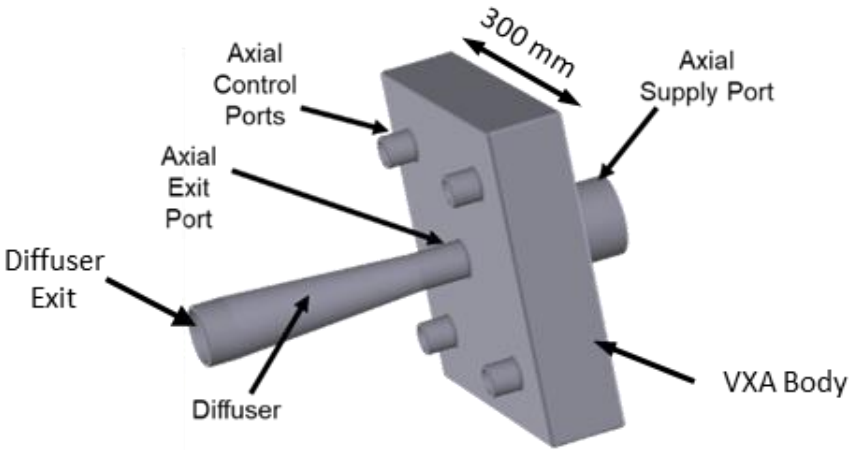

Figure 5 – Historic VXA

The immediate benefit of this VXA design is that all the connecting ports are axial and flow directions are managed by geometries within the VXA body.

The historic VXA consists of four axial control ports distributed around the internal vortex chamber region and is fitted with axial supply and exit ports. It also holds an axial diffusing section at the vortex chamber exit to minimise maximum flow pressure losses. The flows within this historic VXA design are illustrated below. The above VXA has here been termed a 300mm Historic VXA, 300mm being the approximate size of the main VXA body.

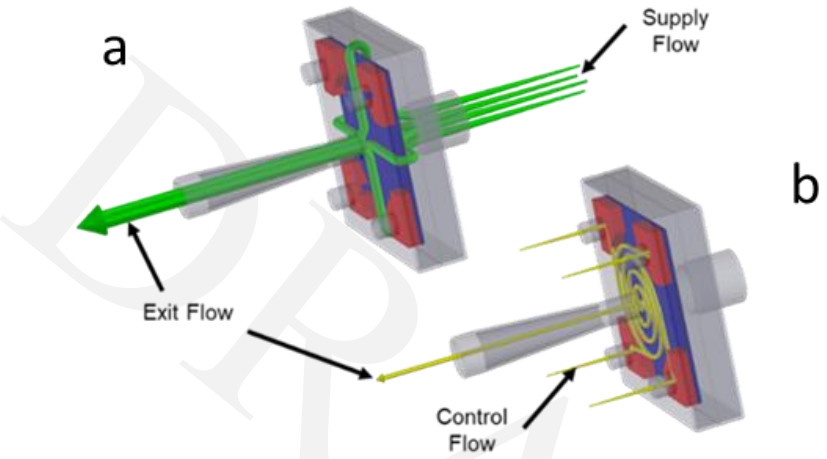

Figure 6 – Historic VXA Supply and Control Flows

Figure 6(a) indicates the maximum supply flow condition during a breach condition and Figure 6(b) a condition of maximum control flow, with no purge flow. These are the extreme ends of the VXA's supply flow characteristic discussed below. Of course, between the above extremes we obtain a combined flow regime illustrated below.

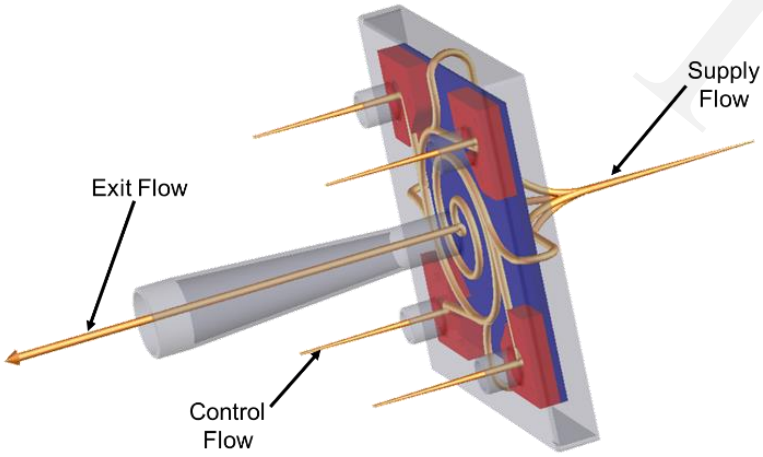

Figure 7 – Historic VXA Combined Supply & Control Flows

At the constant control and exit pressures discussed above the combined flows illustrated in Figure 7 above only vary as a result of the pressure at the supply port, that is within or connected to the glovebox. This supply pressure therefore varies with purge flow provision and ultimately in the final maximum breach condition of a lost glove. This results in a supply pressure vs flow characteristic illustrated below.

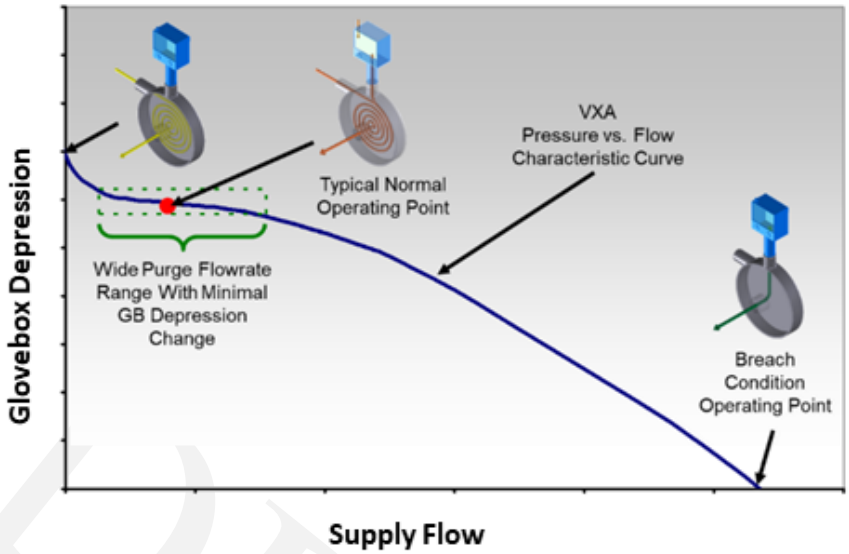

Figure 8 – Typical Historic VXA Characteristic

The simplified VXA characteristic in Figure 8 illustrates the relationship and variation of the glovebox and VXA depression with flow from the glovebox to the ventilation fan. The supply and hence glovebox depression starts at a maximum and falls as the flowrate increases. Figure 8 also illustrates the three flow regimes that were introduced in Figure 3 and Figure 4 above. Figure 8 also identifies an important portion of the VXA characteristic that shows a near constant supply and hence glovebox pressure over a wide range of purge flows. This is an essential feature that must be maintained or extended in future work.

The aim of the above introduction has been to set the scene and provide sufficient background to allow description of the Computation Fluid Dynamic (CFD) modeling exercises that have been conducted, on a model of the historic VXA, using open-source FreeCAD 3D modeling and OpenFoam CFD software.

The objective of this exercise has been to provide a CFD generated characteristic baseline that can be compared with empirically produced measured flow characteristics. If the CFD generated characteristic can be regarded as a true representation of an empirically measured characteristic the CFD model can be regarded as acceptable. The CFD approach can then be used to assess future potential changes to the historic VXA design, that will not be discussed here.

Observations taken from these CFD exercises are introduced and discussed below.

COMPLETE VXA CFD MODELING OBSERVATIONS

Previous exercises, that will not be discussed here, were aimed at assessing the likelihood of using CFD to investigate the possibility of making significant VXA geometry changes at a reduced scale. These CFD assessments were limited to modifications to flow regions within the VXA and resulted in a clearer understanding of the flow performance of changes that could be made.

However, in order to have confidence to take these future steps, it was evident that a clearer understanding of CFD modeling of the historic VXA geometry was required. This has resulted in the complete historic 300mm VXA CFD model discussed below.

These complete historic VXA CFD assessments have provided a 3D model of the physical geometry and its CFD mesh regions. This has resulted in the following, CFD obtained, supply flow characteristic that is compared to a historical, empirically measured, characteristic below.

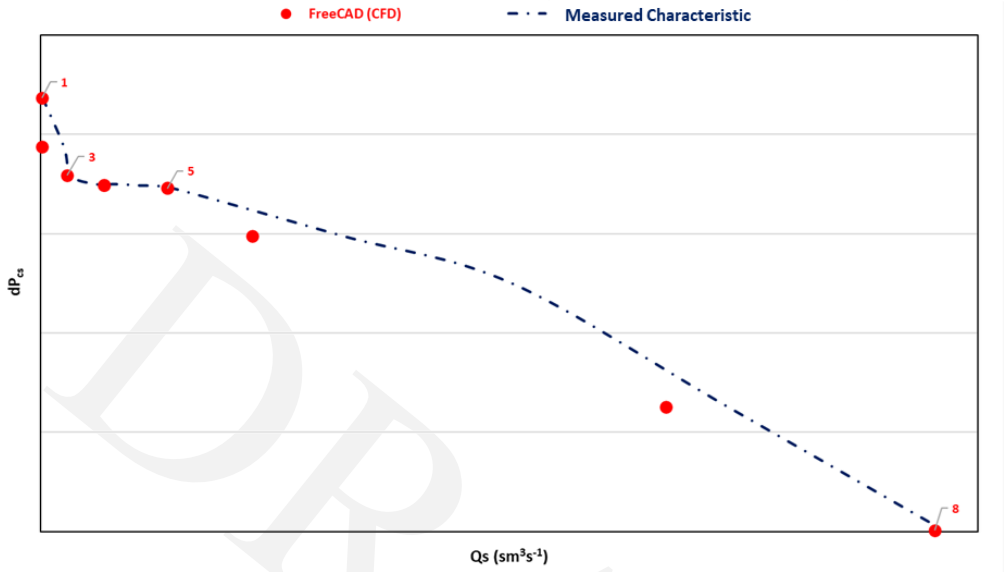

Figure 9 - Historic VXA CFD and Empirical Characteristics

As can be seen in Figure 9, the CFD obtained and measured supply characteristics follow the example shown in Figure 8 above, but a key change is the use of dPcs as the Y axis. This is the pressure difference between the control port entry and the supply port entry, or glovebox interior, that is to be controlled. This allows any changes in control port entry pressure to be accounted for. However, in all of the cases discussed here, the control port has been maintained at atmospheric pressure. The CFD assessments are presented in the eight dPcs steps identified in the FreeCAD (CFD) characteristic.

As will become clear during the CFD observations discussion below, the major parameters that are used to CFD model the measured characteristic of Figure 9 are the pressure boundary conditions at the supply and control port entries and exit port. These boundary conditions allow the model to provide the velocity in the supply port that allows calculation of the supply volumetric flowrate Q_s. These supply flow velocity calculation regions are illustrated below.

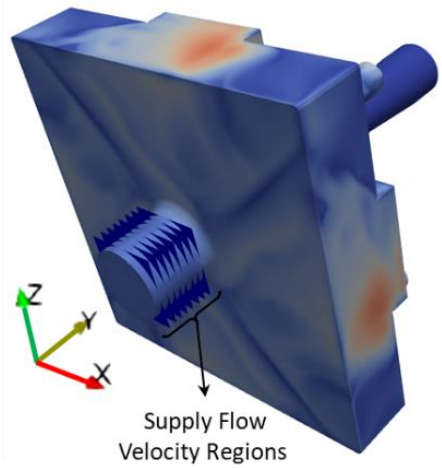

Figure 10 - Supply Flow Velocity Regions

Each of the velocity regions in Figure 10 were defined as arrays of data points to which CFD attributed velocities in the X, Y and Z directions. Supply flows were calculated by identifying the velocity vectors in the Y direction and applying the model's supply port cross sectional area. An average supply velocity and hence supply flow was calculated for each of the velocity regions of Figure 10. At this early stage the numerical assessment was limited to the supply port flowrate introduced above. All other information, to allow visual observation of velocity vectors within the CFD model, was obtained from the two model planes that are illustrated below.

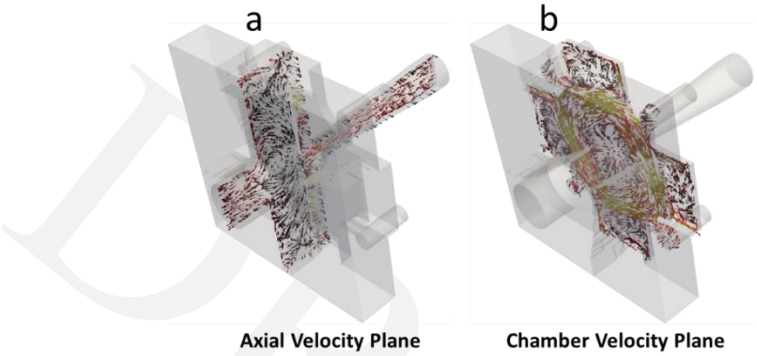

Figure 11 - Axial and Chamber Observation Slices

The two planes identified in Figure 11 were used to make observations from the CFD assessment of each of the four dPcs characteristic steps that are summarised and discussed below.

An important observation must first be made from Figure 9. Steps 01 to 03 cover a far greater dPcs range than Steps 03 to 05 and all lie close to the measured characteristic. The CFD characteristic Steps 03 to 05 Qs values are closely grouped over a far shorter range of dPcs and still lie close to the measured characteristic. This is therefore supporting the important horizontal portion of the measured characteristic that maintains a constant glovebox pressure over a wide range of purge flows.

STEP 01 CHARACTERISTIC OBSERVATIONS

The Step_01 CFD assessment was conducted at a dPcs of 218Pa and resulted in an indicated CFD Figure 10, Y direction Figure 10 velocity region calculated supply flow of 0.000sms^{-1}. The resulting two (Figure 11) model slices are presented below.

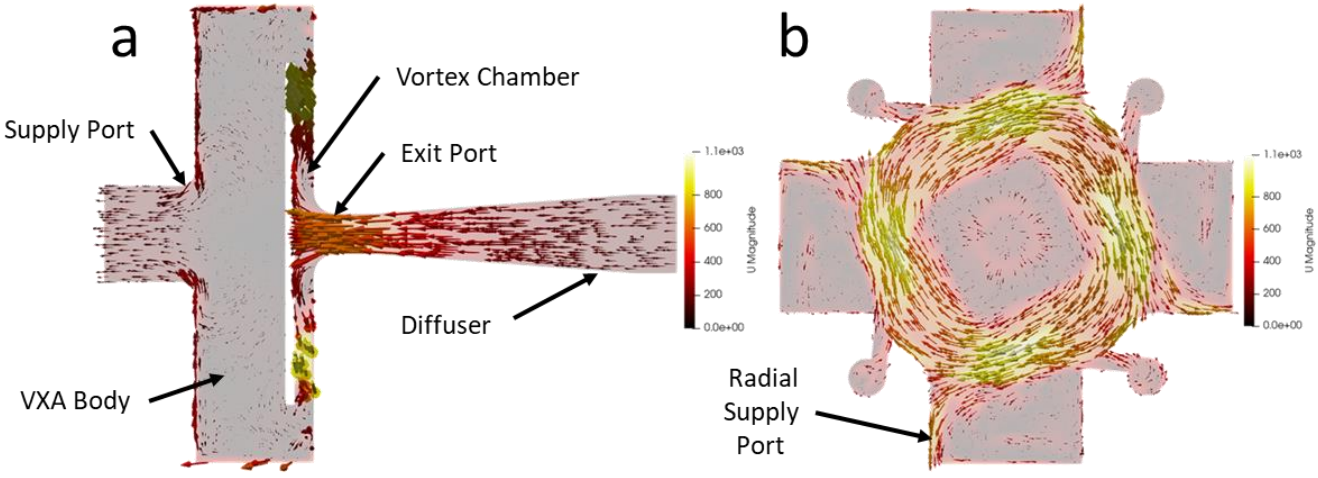

Figure 12 - Step 01 Flow/Velocity Patterns

Figure 12(a) and (b)illustrate the local velocities in the two observation planes, The velocities are scaled and increasing arrow size indicates increased local velocity, at each point plane.

It is immediately clear in Figure 12(b) that the CFD model is confirming that the tangential control flow generated a strong vortex in the periphery of the vortex chamber. Figure 12b also indicates smaller velocities in the radial supply ports and at the vortex chamber centre and exit.

A more detailed illustration, from Figure 12a, provided clearer indications of the Y direction velocities in the axial supply and exit regions is illustrated below.

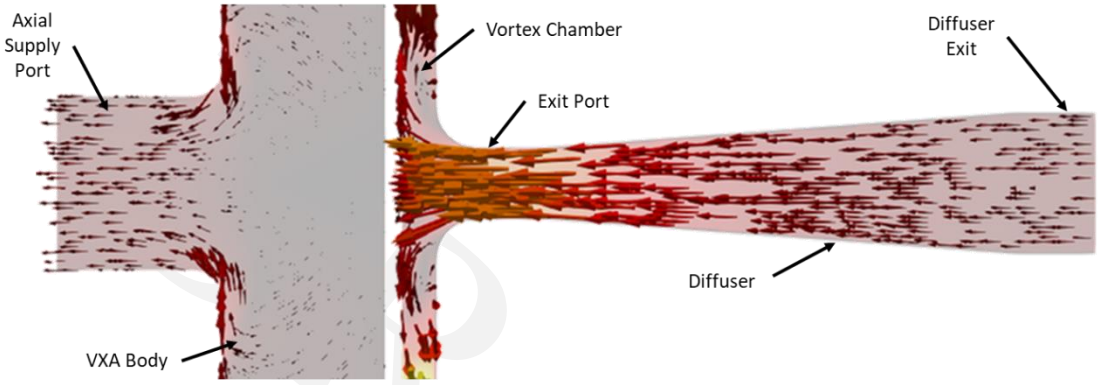

Figure 13 - Supply Port and Exit Port Velocity Patterns

It is clear that Figure 13 is illustrating scaled negative, i.e., from right to left, velocities throughout the VXA. The lowest velocities were indicated in the Supply Port, VXA Body and Diffuser Exit regions of the VXA and the highest in the Vortex Chamber and Exit Port. It is again interesting to note that all velocities are indicated to be negative, i.e., away from the fan. Figure 13 again indicates scaled negative velocities in the supply port, where CFD has numerically reported an average zero velocity and hence flow.

The negative velocities in the vortex chamber exit port and axial diffuser are not unexpected. In this high vortex region of the characteristic, it is expected that the vortex in the vortex chamber can result in a reversed central core flow. The negative scaled velocities in the supply port region are suggesting that alternative representations of the CFD data is required but further work is needed to investigate such alternatives.

The above observations indicated that further investigations were required, and it is therefore suggested that Figure 10 velocity region calculations should be conducted in the VXA control port, the vortex chamber exit port and diffuser exit regions that are identified in Figure 5.

STEP 03 - CHARACTERISTIC OBSERVATIONS

The Step 03 CFD assessment was obtained at a dPcs of 194Pa and resulted in a calculated Figure 10 velocity region supply flow of 0.001sms^{-1}. The Figure 11 model slices are again presented below.

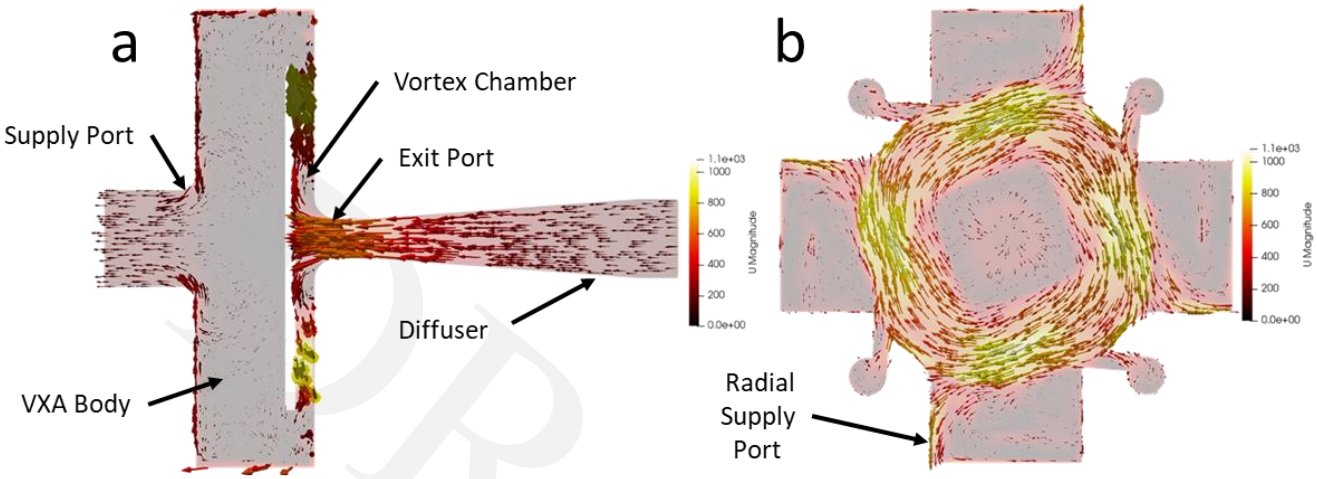

Figure 14 - Step 03 Flow/Velocity Patterns

Once again, the overall observations were that all Figure 14(a) velocities were indicated to be negative and the strong vortex is again concentrated at the periphery of the vortex chamber in Figure 14(b).

STEP 07 - CHARACTERISTIC OBSERVATIONS

Step 07 CFD assessment was obtained at a dPcs of 179Pa and resulted in an increased calculated model supply flow of 0.007sms^{-1}. The scaled Figure 11 model slices are again presented below.

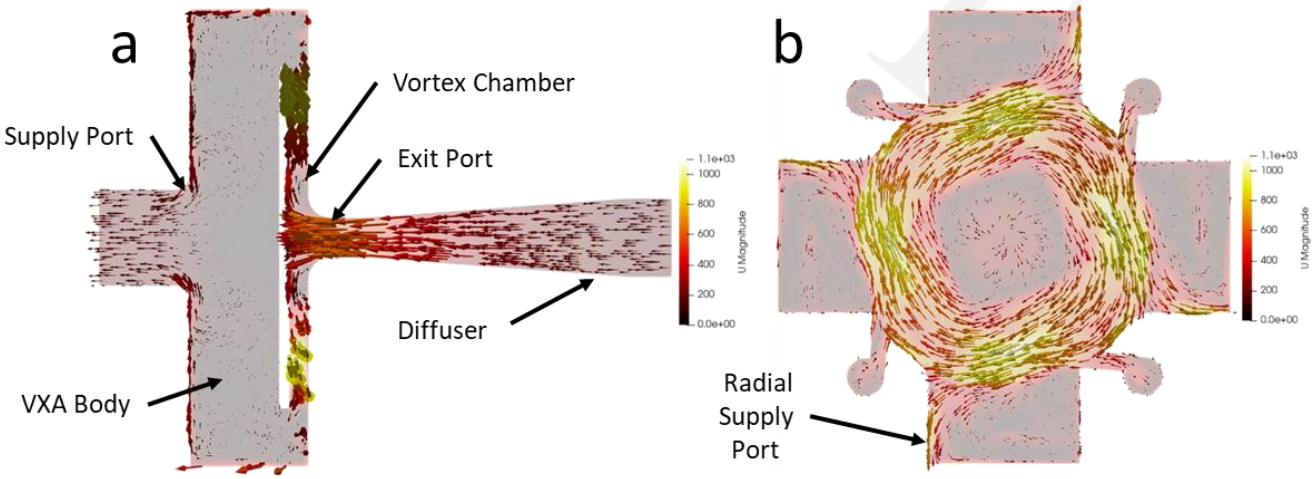

Figure 15 - Step 03 Flow/Velocity Patterns

Once again, Figure 15(a) and (b) suggested that all indicated velocities were negative. Initial observations also suggested there seemed to be no change in the velocity patterns between Step_03 and Step_07. However, a very close inspection confirmed that there were indeed small changes, as may be expected due to the very small decrease in dPce over this near horizontal portion of the characteristic. The only major change was therefore the increase in the Figure 10

velocity region calculated supply flows from 0.001sms^{-1}, at Step_03, to 0.007sms^{-1}. A more detailed illustration of velocities in the supply and exit regions is again shown below.

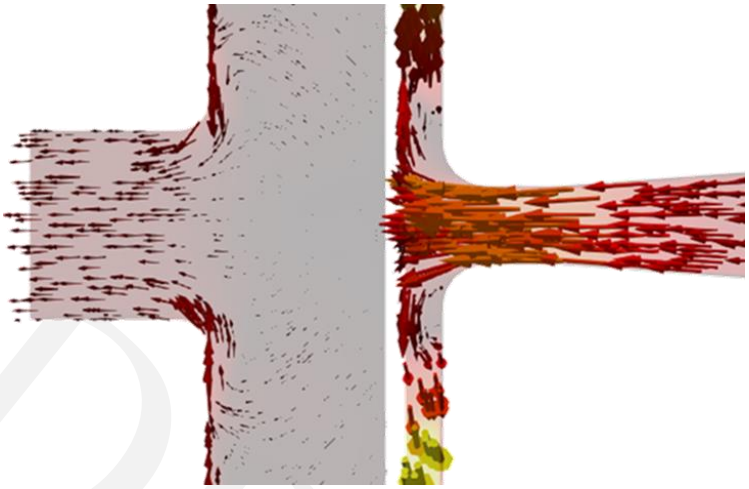

Figure 16 – Step_07 Supply Port and Exit Port Velocity Patterns

Once again, from Figure 16**Error! Reference source not found.**, there is no indication of the calculated Figure 10 supply port velocity region positive velocities and hence flows. Again confirming that further interpretation is required.

STEP 08 - CHARACTERISTIC OBSERVATIONS

Following the above observations of Steps 01 to 07 it was of interest, for these preliminary observations, to move from the high vortex low supply flow portion of the characteristic to the opposite, low vortex high supply flowrate position of the VXA characteristic, i.e., the Breach condition. These Step_08 observations were obtained at a dPcs of 0.722Pa resulting in a Figure 10 velocity region calculated supply flow of 0.051sms^{-1} that, as can be seen in Figure 9, was again very close to the expected Step_08 measured supply flow.

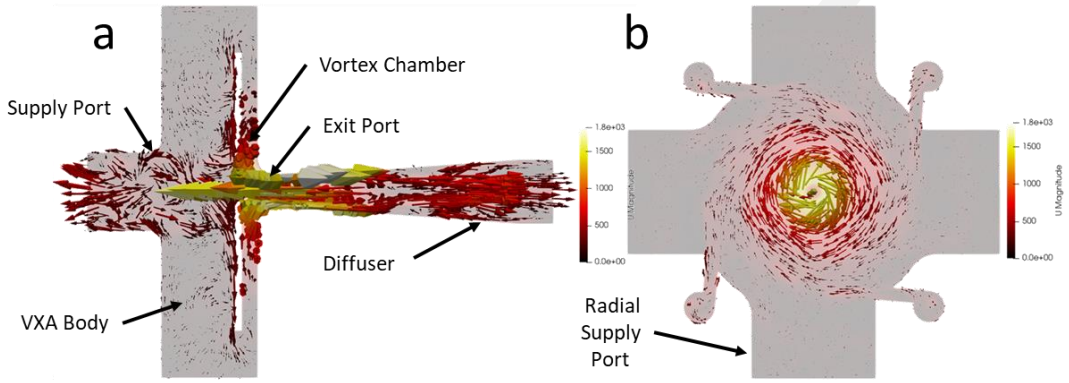

Figure 17 - Step 09 Flow/Velocity Patterns

Once again, Figure 17(a) suggested that indicated velocities were still generally negative and indeed greater in the supply port and exit port regions that are illustrated in greater detail below. As indicated in Figure 17b, the strong vortex region was moved to the centre of the vortex chamber with no indication of any reverse flow generation in the radial supply ports.

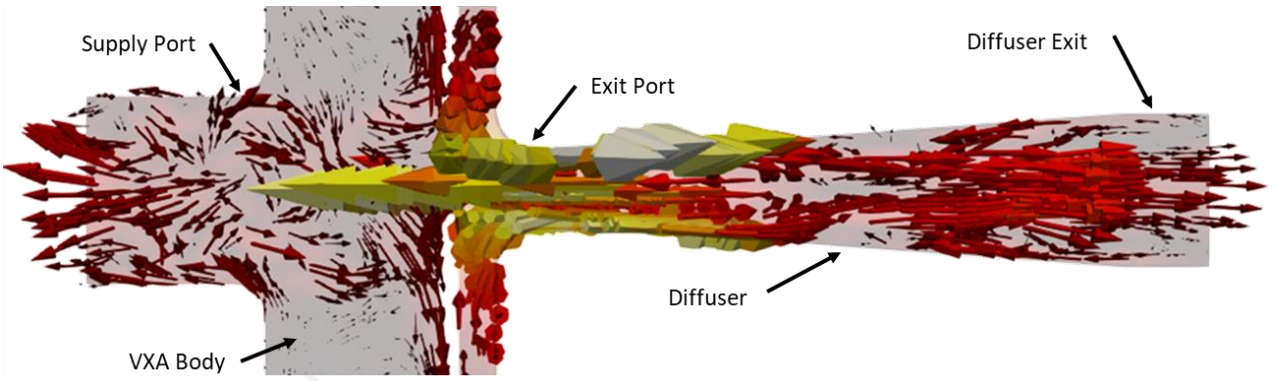

Figure 18 - Step_08 Supply Port and Exit Port Velocity Patterns

It is very difficult to interpret the details of the velocity patterns in Figure 18 because a clearer understanding of the velocity scaling impacts is required. However, although further assessment and analysis is required, it was helpful to make some observations for this preliminary note.

An immediate observation was the larger increase in negative flow in the left-hand central supply port region. But it was also clear that Step_08 had indicated generally increased positive velocities between the supply port and VXA body. These positive velocities also seem to have resulted in positive radial flows at the right had wall of the VXA body. This is therefore supporting the expected increased positive supply port velocity and hence flow.

The reversed vortex core velocity in the exit port had increased but there was clearly a greatly increased positive exit flow before and in the diffuser and exit sections of Figure 18. All these observations therefore supported the dramatically increased Step_08 supply flow of 0.0051sms^{-1}.

These increased velocities were also indicated to be present in the vortex chamber and exit port region of Figure 17b that is illustrated in greater detail below.

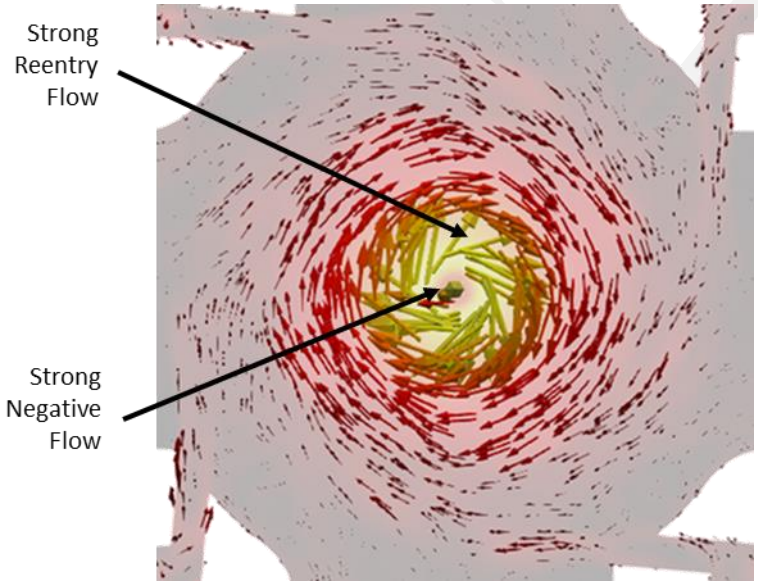

Figure 19 – Step_08 Vortex Chamber and Exit Port Velocity Pattern

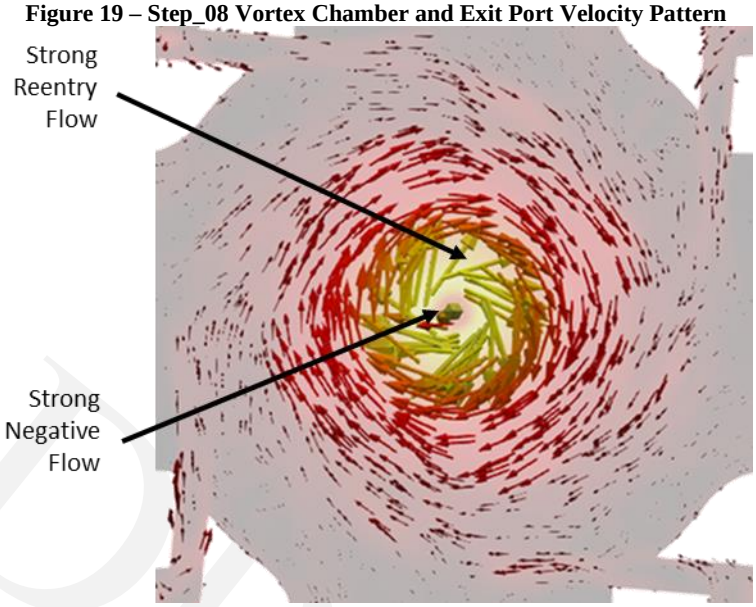

Figure 19 Figure 19 vortex chamber and exit port velocity patterns illustrate further changes that must be expected at this extreme position in VXA characteristic. Although the vortex chamber peripheral vortex scaled velocities were significantly reduced, the vortex was maintained, and the stronger vortex region is now indicated to have been moved to the central vortex chamber exit port region.

Observations from Figure 19 also suggested that there was a strong negative flow within the central exit port region. There was also a clear indication of a negative flow from the center of the exit port into the vortex chamber that is forced into a vortex. This stronger central vortex may again be generated by the reversed exit core vortex that has re-entered the exit port. This observation may also be supported by the large positive peripheral velocities visible in the exit port in Figure 18.

Once again, further interpretation tasks and skills are required to draw firmer conclusions from the Step_01 to 08 observations. But the clear agreement with the measured characteristic in Figure 9 and the preliminary observations obtained from the above velocity patterns must offer some support to the acceptability of the CFD modeling conducted here.

CFD OBSERVATION DISCUSSION

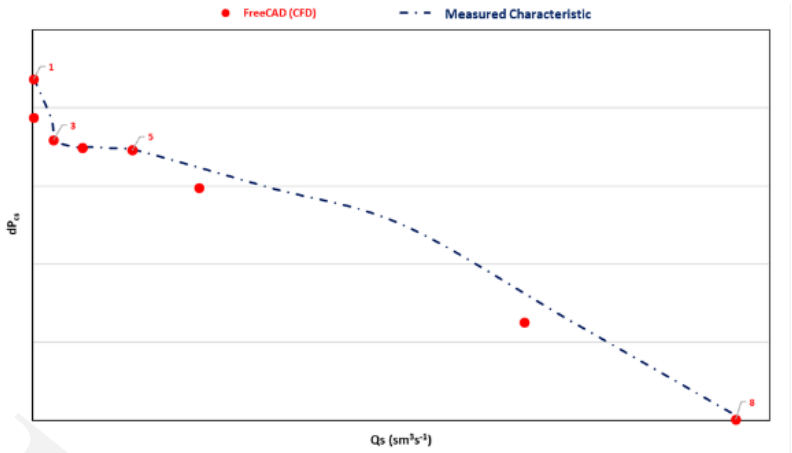

The major positive result obtained from CFD modeling of a complete historic VXA was the generation of a flow characteristic that was found to lie close to the trusted empirically measured characteristic.

The first CFD characteristic points, Steps_01 to 05, were seen to agree with and lie very close to the measured characteristic. This was also the case for the final Step_08 point but two intermediate points were further away from the measured characteristic. Although providing confidence in the adopted modeling method it was clear that further work was required to either make modeling or data interpretation changes. It is felt that investigations into the scaling approach of the data handling software is required. One concern was that small negative velocities indicated in the supply port and diffuser exit may actually be close to zero, but still represented by the small scaled negative vectors. This result led to interest into further visual observations of CFD the model generated velocity vector patterns.

Velocity vector patterns generated from a series of five CFD model cases that provided key points on the CFD flow characteristic were obtained. Observations from each of the five key CFD model cases discussed above are briefly summarised below.

CFD Step_01

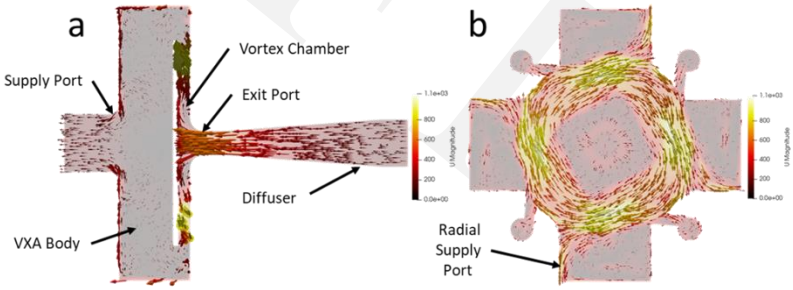

The velocity patterns from Step_01, at the left hand zero-supply flow point of the characteristic introduced a potential disagreement between the CFD velocity regions calculated supply port flow value of 0.000sm^{3}s^{-1} and the clear observation that only negative flows were visible throughout the device in Figure 12. The calculated zero supply flow was also supported by the position on the characteristic, but there was no apparent reason how the observed negative supply port velocities could be produced.

A negative flow in the chamber exit and diffuser section was explained due the likelihood of a reversed central core flow generated by the vortex. But it is not clear how this negative flow could be transmitted to the supply port and not observed by the supply flow calculations. The only indication of negative flows in the radial supply ports was a small region that seems to be generated by the impacting tangential control flows.

CFD Step_03

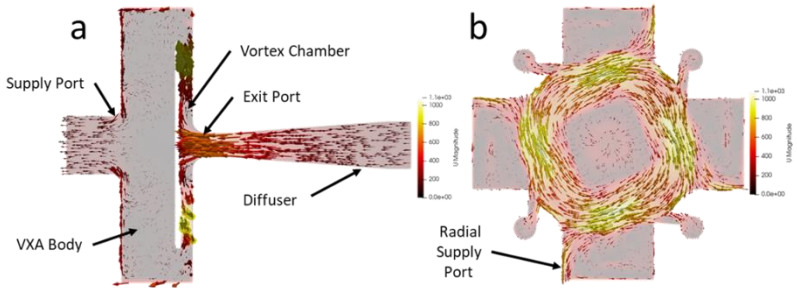

Step_03 again suggested an overall indication of negative flow throughout the device. The slight increase in calculated velocity regions supply flow of $0.001sm^3s^{-1}$ supported the observed minor changes in the velocity patterns. Close examination of the velocity vector patterns confirmed that small changes were observable. Once again, the only suggestion of negative flow in the radial supply ports were those introduced by the tangential control flow.

CFD Step_07

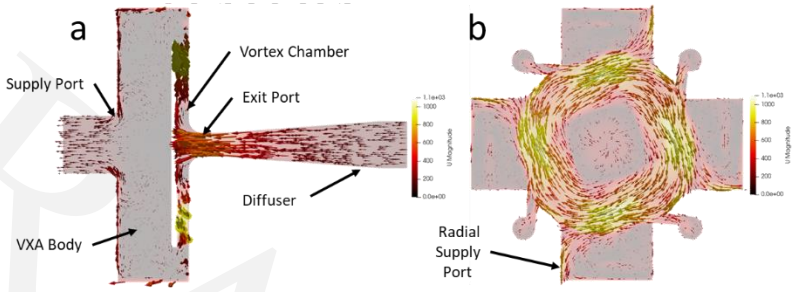

Once more, at this final position of the strong vortex horizontal region of the VXA characteristic, the Step_07 velocity regions calculated supply flow increase to $0.007sms^{-1}$ and the velocity patterns again suggested few changes from the previous velocity patterns and still negative flows throughout. The only negative radial supply port velocities were again from the tangential control flow.

CFD Step_09

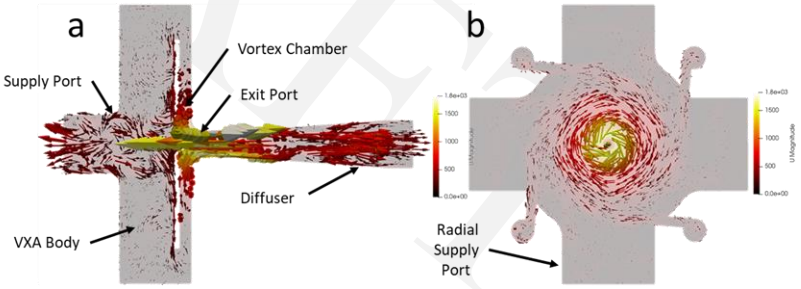

The Step_09 maximum velocity regions supply, breach, flow of $0.051sms^{-1}$ resulted in many changes to observations made from the velocity patterns.

Although reverse velocities in the supply port entry and exit port were observed to have increased it was also clear that there were positive velocities indicated from the supply port into the VXA body, in the periphery of the exit port and through a major portion of the diffuser and diffuser exit. A further major change was the concentration of the vortex at the vortex chamber exit and a clear indication that there were strong central velocities suggesting recirculation in the chamber exit port.

The Step_09 observations clearly supported the breach flow position on the measured characteristic and hence the calculated velocity regions positive supply flow of $0.051sms^{-1}$. This result is confirming the need to obtain a greater understanding of the data handling software's approach to velocity scaling and the implications on observations.

The above observations of changes from negative to positive velocity vectors and hence flows have resulted in the identification of a need to conduct velocity region calculations of the VXA control entry, vortex chamber and diffuser exit ports, illustrated in Figure 5.

CONCLUSIONS

1. The overall conclusion must be that current CFD VXA modeling has provided a clear indication that the model can reproduce the known, empirically measured, VXA flow characteristic
2. The CFD model provided a flow characteristic that echoed the supply flows and pressures of the measured characteristic very closely in most cases, but several points deviated from the measured cases and require further investigation
3. The method used to illustrate and observe scaled velocities within the CFD model resulted in concerns regarding the generation of negative velocities and hence flows that cannot currently be explained
4. A greater understanding of scaled velocities is required in order to obtain clearer observations of small negative velocity vectors in regions where velocity calculations have indicated positive velocities and hence flows
5. Further CFD assessments are require investigating velocities and hence flows at the control inlet, vortex chamber and diffuser exits